Available online at www.sciencedirect.com
SCIENCE DIRECT®
Journal of Solid State Chemistry 178 (2005) 3101–3109
JOURNAL OF SOLID STATE CHEMISTRY
www.elsevier.com/locate/jssc

Structure, magnetic properties and ^{119}Sn Mössbauer spectroscopy of PrRhSn

Kazimierz Łątka[a], Roman Kmieć[b], Jacek Gurgul[c], Michał Rams[a], Andrzej W. Pacyna[b], Tobias Schmidt[d], Rainer Pöttgen[d,*]

[a]*Marian Smoluchowski Institute of Physics, Jagiellonian University, Reymonta 4, Kraków 30-059, Poland*
[b]*Henryk Niewodniczański Institute of Nuclear Physics, Polish Academy of Sciences, Radzikowskiego 152, Kraków 31-342, Poland*
[c]*Institute of Catalysis and Surface Chemistry, Polish Academy of Sciences, Niezapominajek 8, Kraków 30-239, Poland*
[d]*Institut für Anorganische und Analytische Chemie, Universität Münster,Corrensstrasse 36, Münster D-48149, Germany*

Received 1 June 2005; received in revised form 22 June 2005; accepted 28 June 2005
Available online 18 August 2005

Abstract

PrRhSn was synthesized in polycrystalline form by a reaction of praseodymium, rhodium, and tin in an arc-melting furnace. The sample was investigated by powder and single crystal X-ray diffraction: ZrNiAl type, space group $P\bar{6}2m$, $a = 742.49(7)$, $c = 415.05(5)$ pm, w$R_2 = 0.0737$, 353 F^2 values and 14 variables. The PrRhSn structure has two crystallographically independent rhodium sites with a tricapped trigonal prismatic coordination, i.e. [Rh1Sn$_3$Pr$_6$] and [Rh2Sn$_6$Pr$_3$]. The rhodium and tin atoms build up a three-dimensional [RhSn] network with short Rh–Sn contacts (278 and 285 pm), in which the praseodymium atoms fill distorted hexagonal channels. The magnetic and electronic properties of PrRhSn have been studied by means of AC and DC magnetic susceptibility measurements as well as ^{119}Sn Mössbauer spectroscopy. A transition from a paramagnetic to a ferromagnetic state was found at $T_C = 3.0$ K.

Keywords: Intermetallic compound; Magnetism; Mössbauer spectroscopy

1. Introduction

The rare-earth metal based stannides *RE*RhSn (*RE* = rare-earth element) have thoroughly been investigated in recent years [1–5, and references therein]. A detailed literature overview is given in [1] and [5]. Especially, the valence fluctuations of CeRhSn and the heavy fermion behavior of YbRhSn are of great interest.

The crystal chemistry and the physical properties of the *RE*RhSn stannides with the early rare-earth elements have controversially been discussed. The lattice parameters for CeRhSn, PrRhSn, and NdRhSn reported by Routsi et al. [6] are different from those reported by Mishra et al. [1]. A recent single crystal study of the NdRhSn structure [7] clearly confirmed the X-ray powder data given in [1]. The two different studies also revealed a discrepancy concerning the magnetic ordering. While no hint for magnetic ordering was evident in the original work [6], ferromagnetic ordering at $T_C = 10.3$ K was clearly detected on the basis of magnetization and ^{119}Sn Mössbauer spectroscopic studies [7].

In the course of our systematic studies on structure-property relations of *RE*RhSn stannides we have now investigated the praseodymium compound in more detail. The crystal structure, the magnetic properties and temperature dependent ^{119}Sn Mössbauer spectroscopic data of PrRhSn are reported herein.

*Corresponding author. Fax: +49 251 83 36002.
E-mail addresses: pottgen@uni-muenster.de, uflatka@cyf-kr.edu.pl (R. Pöttgen).

0022-4596/$ - see front matter © 2005 Elsevier Inc. All rights reserved.
doi:10.1016/j.jssc.2005.06.041

2. Experimental

2.1. Synthesis

Starting materials for the synthesis of PrRhSn were praseodymium ingots (Johnson Matthey, distilled lumps), rhodium powder (Degussa-Hüls, 200 mesh), and tin granules (Heraeus), all with purities better than 99.9%. The larger praseodymium lumps were first cut under paraffin oil into smaller pieces, washed with *n*-hexane, and kept in Schlenk tubes. The paraffin oil and *n*-hexane have been dried over sodium wire. A small praseodymium piece was then arc-melted to a small button under an argon pressure of ca. 600 mbar. The argon was purified before over titanium sponge (900 K), silica gel, and molecular sieves. The praseodymium button was subsequently mixed with a cold-pressed pellet (∅ 6 mm) of rhodium powder and pieces of the tin granules in the ideal 1:1:1 atomic ratio and placed in the water-cooled copper crucible of the arc-melting chamber [8]. The three elements were then arc-melted under an argon pressure of ca. 800 mbar. The product button was remelted three times to ensure homogeneity of the sample. The total weight loss after the four melting procedures was smaller than 0.5 weight-%. The sample was obtained in X-ray pure form in an amount of 1 g. The PrRhSn sample is stable in moist air over months in compact form as well as a polycrystalline powder.

2.2. X-ray diffraction

The arc-melted sample was analyzed through a Guinier powder diagram using Cu$K\alpha_1$ radiation and α-quartz ($a = 491.30$, $c = 540.46$ pm) as an internal standard. The lattice parameters (Table 1) were obtained from a least-squares fit of the powder data. The correct indexing was ensured through an intensity calculation [9] taking the atomic positions from the structure refinement. The lattice parameters determined from the powder and the single crystal agreed well.

Single crystal intensity data were collected at room temperature by use of a four-circle diffractometer (CAD4) with graphite monochromatized Mo$K\alpha$ (71.073 pm) radiation and a scintillation counter with pulse height discrimination. The scans were taken in the $\omega/2\theta$ mode and an empirical absorption correction was applied on the basis of psi-scan data, followed by a spherical absorption correction. All relevant details concerning the data collection are listed in Table 1.

2.3. Structure refinement

Irregularly shaped single crystals of PrRhSn were examined by use of a Buerger camera equipped with an image plate system (Fujifilm BAS–1800) in order to establish suitability for intensity data collection. The isotypy with the hexagonal ZrNiAl type [10–12], space group $P\bar{6}2m$, was already evident from the X-ray powder data.

Table 1
Crystal data and structure refinement for PrRhSn

Empirical formula	PrRhSn
Molar mass (g/mol)	362.51
Unit cell dimensions	$a = 742.49(7)$ pm
(Powder data)	$c = 415.05(5)$ pm
	$V = 0.1982$ nm^3
Calculated density (g/cm^3)	9.11
Crystal size (μm^3)	$20 \times 20 \times 90$
Transm. ratio (max/min)	2.04
Abs. coefficient (mm^{-1})	33.3
F(000)	462
θ range for data collection	3–35°
Range in hkl	±10, ±10, ±6
Total no. of reflections	760
Independent reflections	353 ($R_{int} = 0.0420$)
Reflections with $I > 2\sigma(I)$	326 ($R_{sigma} = 0.0488$)
Data/parameters	353/14
Goodness-of-fit on F^2	1.079
Final R indices [$I > 2\sigma(I)$]	$R_1 = 0.0322$; w$R_2 = 0.0715$
R indices (all data)	$R_1 = 0.0384$; w$R_2 = 0.0737$
Flack parameter	−0.09(6)
Extinction coefficient	0.022(2)
Largest diff. peak and hole	2.66 and −1.82 e/Å^3

The atomic parameters of isotypic TmRhSn [1] were taken as starting values and the structure was refined using SHELXL-97 [13] (full-matrix least-squares on F^2) with anisotropic atomic displacement parameters for all atoms. Refinement of the correct absolute structure was ensured through a refinement of the Flack parameter [14,15]. As a check for the correct composition and the correct site assignment the occupancy parameters were refined in a separate series of least-squares cycles along with the displacement parameters. All sites were fully occupied within two standard deviations and in the final cycles the ideal occupancies were assumed again. The final difference Fourier synthesis was flat (Table 1). The positional parameters and interatomic distances of the refinement are listed in Tables 2 and 3. Further details on the structure refinement are available.[1]

2.4. Scanning electron microscopy

The single crystal (coated with a carbon film) and the bulk sample have been analyzed in an LEICA 420 I scanning electron microscope equipped with an OXFORD EDX analyzer. PrF_3, rhodium, and tin have been used as standards. The analyses (32±2 at% Pr : 33±2 at% Rh : 35±2 at% Sn) were in good agreement with the

[1]Details may be obtained from: Fachinformationszentrum Karlsruhe, D-76344 Eggenstein-Leopoldshafen (Germany), by quoting the Registry No. CSD–415370.

Table 2
Atomic coordinates and anisotropic displacement parameters (pm^2) for PrRhSn

Atom	Wyckoff site	x	y	z	U_{11}	U_{22}	U_{33}	U_{12}	U_{eq}
Pr	3*f*	0.41460(15)	0	0	72(3)	79(5)	58(4)	39(2)	69(3)
Rh1	2*d*	1/3	2/3	1/2	89(5)	U_{11}	77(8)	45(2)	85(4)
Rh2	1*a*	0	0	0	74(6)	U_{11}	111(10)	37(3)	53(4)
Sn	3*g*	0.75196(16)	0	1/2	63(4)	72(5)	52(5)	36(3)	61(3)

Note: U_{eq} is defined as one-third of the trace of the orthogonalized U_{ij} tensor. $U_{13} = U_{23} = 0$.

Table 3
Interatomic distances (pm), calculated with the lattice parameters taken from X-ray powder data of PrRhSn

Pr:	4	Rh1	305.0	Rh1:	3	Sn	284.5
	1	Rh2	307.8		6	Pr	305.0
	2	Sn	325.3	Rh2:	6	Sn	277.5
	4	Sn	339.2		3	Pr	307.8
	4	Pr	387.2	Sn:	2	Rh2	277.5
	2	Pr	415.1		2	Rh1	284.5
					2	Sn	319.0
					2	Pr	325.3
					4	Pr	339.2

Note: All distances within the first coordination sphere are listed. Standard deviations are all smaller or equal than 0.2 pm.

equiatomic composition. The relatively large standard deviation accounts for the various point analyses. No impurity elements have been observed.

2.5. Magnetic measurements

Detailed magnetic investigations were made in AC and DC modes using the polycrystalline PrRhSn sample. The DC magnetization data were collected using a SQUID magnetometer MPMS XL5 (Quantum Design) in a wide temperature range 1.9–300 K with a static field $H_0 = 1$ kOe. The field dependence of the magnetization was registered at $T = 2$ K. The maximum external magnetic field used in this experiment reached 50 kOe.

The bulk AC magnetic susceptibility measurements were undertaken employing a Lake Shore 7225 susceptometer operating in the temperature range 2.1–5.0 K. The in-phase $\chi'(\omega)$ and out-phase $\chi''(\omega)$ components were recorded simultaneously as a function of temperature with an internal frequency $f = 125$ Hz and the oscillating field strength $H_{AC} = 1$ Oe. Zero-field cooled DC susceptibility was measured over the 2.3–7.5 K temperature range in a static field $H_0 = 50$ Oe.

2.6. ^{119}Sn Mössbauer spectroscopy

Mössbauer spectra of PrRhSn were obtained by means of the 23.875 keV resonance transition of ^{119}Sn. Experiments were made with a spectrometer of conventional design and a liquid helium cryostat. The velocity scale was calibrated with a ^{57}Co(Rh) source and a metallic iron foil at room temperature. The $Ba^{119m}SnO_3$ source was kept close to 4.2 K while the temperature of the absorber was varied between 1.95 K and room temperature. Special care was taken to optimize the absorber thickness by Czjzek's method [16] based on numerical solution of the equation obtained from the condition to get maximal value of the ratio of observed effect to experimental error. The γ-rays were detected using a 3 cm thick NaJ(Tl) scintillation counter. A palladium foil of 0.05 mm thickness was used as a critical absorber for tin X-rays to reduce the background intensity of the recorded spectra.

Since the tin positions in the ZrNiAl type structure of PrRhSn have a low site symmetry (*m*2*m*), a full hyperfine interaction Hamiltonian [17] within the Lorentz approximation was applied to analyze the magnitudes of the hyperfine parameters. The following parameters were least-squares fitted to the resonance spectra: the isomer shift δ_{IS}, the quadrupole coupling constant $\Delta E_Q = eQV_{zz}$, θ and φ angles which define the direction of the magnetic hyperfine field H_{hf} with respect to the main axis of the electric field gradient (EFG) tensor and the asymmetry parameter $\eta = (V_{xx} - V_{yy})/V_{zz}$ $(0 \leqslant \eta \leqslant 1)$. Resonance spectra of PrRhSn at low temperatures show some broadening of the resonance lines caused by the distribution of H_{hf}. To take this into account, the Wivel and Mørup approach [18] was used. Then, the spectra were least-squares fitted with 60 values of H_{hf}, giving the probability distribution curve $F(H_{hf})$.

3. Results and discussion

3.1. Crystal chemistry

The crystal chemistry of the *RE*RhSn stannides with the ZrNiAl type structure [10–12] has already been discussed in detail [1]. The main point for the praseodymium compound is the discrepancy in the lattice parameters between those reports by Routsi et al. [6] and Mishra et al. [1]. The present structure refinement

revealed fully occupied sites and full rhodium–tin ordering, and the single crystal lattice parameters ($a = 740.95(7)$, $c = 414.45(10)$ pm) are in good agreement with the X-ray powder data determined in our previous investigation [1]. Thus, the PrRhSn sample investigated here has the stoichiometric composition. The deviation in the lattice parameters observed in [6] most likely results from a different sample composition or a homogeneity range. This might also explain the different magnetic data.

The PrRhSn structure contains two crystallographically independent rhodium sites in a tri-capped trigonal prismatic coordination. The shortest interatomic distances occur between the rhodium and tin atoms (278 and 285 pm). These distances are only slightly longer than the sum of the covalent radii of 265 pm for rhodium and tin [19]. Together, the rhodium and tin atoms build up a three-dimensional [RhSn] network in which the praseodymium atoms fill distorted hexagonal channels. The coordination number for the praseodymium atoms is 17 (6 Pr + 5 Rh + 6 Sn). For drawings of the hexagonal *RE*RhSn structures and further details concerning the crystal chemistry of the *RE*RhSn stannides we refer to [1] and [5].

3.2. Magnetic properties

The temperature dependence of the zero-field cooled DC inverse susceptibility is presented in Fig. 1. The data for $\chi(T)$ above 100 K closely obey a modified Curie–Weiss formula: $\chi = \chi_0 + N_A\mu_0(\mu_B\mu_{eff})^2/3k_B(T-\theta_P)$. The following parameters were extracted from the fitting procedure: the temperature independent factor $\chi_0 = 6.5(7)\times10^{-7}\,cm^3/g$, the paramagnetic Curie temperature $\theta_P = 2.9(6)$ K and the effective magnetic moment $\mu_{eff} = 3.64(3)\mu_B$ which is only slightly larger than the theoretical value for a free Pr^{3+} ion described by $\mu_{eff} = g\mu_B[J(J+1)]^{1/2} = 3.58\,\mu_B$. The other symbols in the above equation have their usual meaning. The positive value of θ_P indicates the predominance of ferromagnetic exchange interactions. As was expected there is no magnetic moment localized on the rhodium atoms [7,20]. Low temperature inverse susceptibility shows a tendency to flatten (see inset of Fig. 1), what can be ascribed to ferrimagnetic ordering.

Fig. 2 presents the magnetization (in μ_B per formula unit) as a function of the magnetic field at 2 K, i.e. below the Curie temperature. The magnetization curve does not saturate even at $H = 50$ kOe, but a near saturation effect is seen with an extrapolated $(1/H\to0)$ moment of 1.85(2) μ_B/Pr. The latter is far below the maximal value of 3.20 μ_B/Pr according to the theoretical moment gJ. However, one should not forget here that this moment has been derived from magnetization measurements made on a polycrystalline sample, what can play an essential role, since magnetic anisotropy in praseodymium intermetallics is usually significant. The hysteresis loop (see inset of Fig. 2) is very narrow but one has to keep in mind that the temperature of the measurement ($T = 2$ K) is close to the ordering temperature $T_C = 3.0$ K. The coercive field is about 20(2) Oe and the remanence is equal to 0.023(1) μ_B/f.u.

The temperature variation of the ZFC mass susceptibility measured at a static field $H_0 = 50$ Oe is presented in Fig. 3. The Curie temperature of $T_C = 3.0(1)$ K was determined from the minimum of the derivative $d\chi/dT$ (see inset of Fig. 3). This temperature corresponds to the inflection point of the ZFC susceptibility curve.

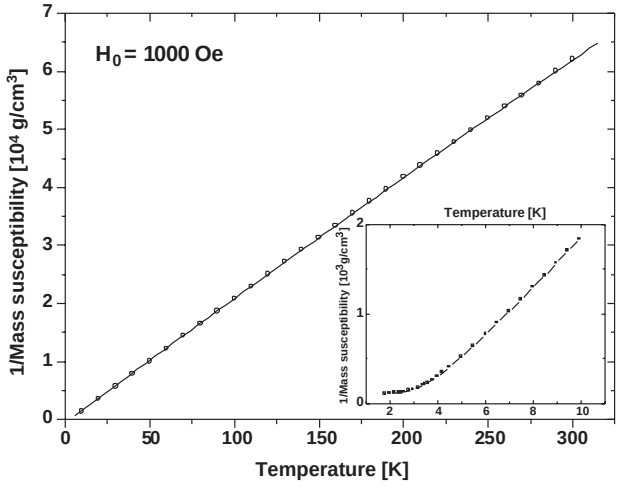

Fig. 1. Temperature dependence of the zero-field cooled (ZFC) reciprocal mass susceptibility of PrRhSn recorded in an external magnetic field of $H_0 = 1000$ Oe, where the solid line is a result of the fitting procedure in the paramagnetic range. The inset displays low-temperature inverse mass susceptibility of PrRhSn limited to the temperature range 1.9–10 K (extended scale).

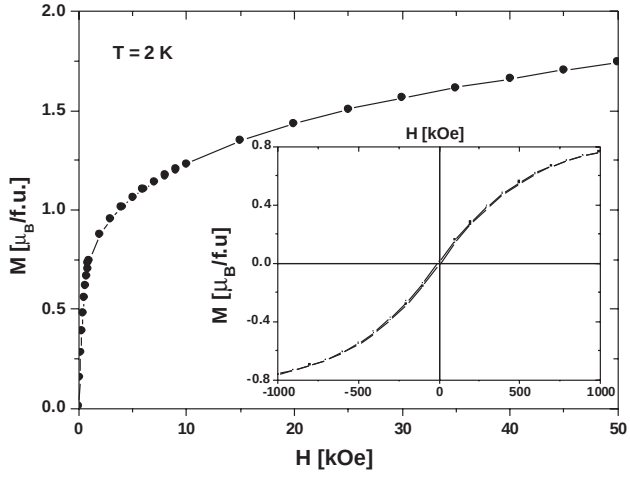

Fig. 2. Virgin magnetization vs. external magnetic field for PrRhSn at $T = 2$ K as obtained after ZFC process. The inset shows the small hysteresis loop of the mass magnetization.

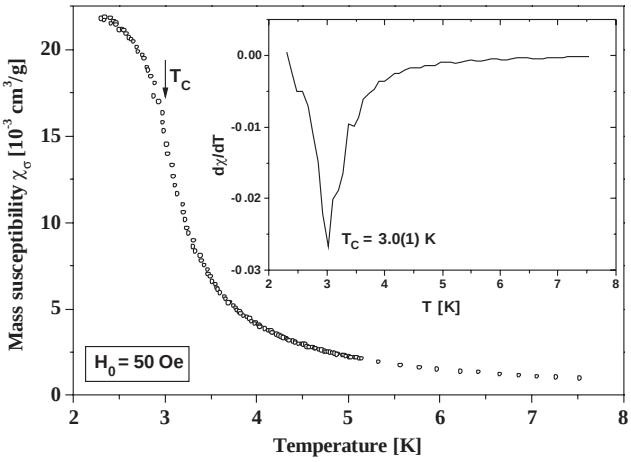

Fig. 3. Temperature dependence of the zero-field cooled (ZFC) DC mass susceptibilitiy of PrRhSn measured in a static field of $H_0 = 50$ Oe.The inset displays the derivative $d\chi/dT$, which has a sharp minimum at $T_C = 3.0(1)$ K.

In order to get more information about the character of the observed transition, AC susceptibility measurements were performed. This method was chosen because it enables investigations with very small amplitudes of the oscillating fields H_{AC} not significantly affecting the magnetic system and therefore is well suited for a precise determination of magnetic phase transitions and their dynamics. The results of the AC susceptibility $\chi = \chi' - i\chi''$ measurements for PrRhSn are shown in Fig. 4. Both the real and imaginary parts of the AC susceptibility show a strong peak near the Curie temperature. One can note that the position of the real part maximum located at $T_{max}(\chi') = 2.8(1)$ K agrees within limits of experimental error with the above obtained Curie temperature $T_C = 3.0(1)$ K.

3.3. ^{119}Sn Mössbauer spectroscopy

The ^{119}Sn Mössbauer studies of PrRhSn were performed in the temperature range 1.95–300 K (Fig. 5). The non-cubic local symmetry at the tin sites (*m*2*m*) leads to resonance spectra with a non-vanishing quadrupole splitting. High-temperature spectra i.e., in the paramagnetic range, were fitted as typical quadrupole doublets with an additional small impurity component. The averaged hyperfine parameters of the unknown phase are as follows: $|\Delta E_Q|^{tr} = 2.33(1)$ mm/s, $\delta_{IS}^{tr} = 1.88(2)$ mm/s and $\Gamma^{tr} = 0.85(5)$ mm/s. The total absorption area of an additional phase is about 10%, although the Guinier powder pattern revealed single phase PrRhSn. It is worth noting that the absorption area of the unknown phase remained unchanged through the whole temperature range and was extracted from the fitting procedure of the low-temperature spectra.

The magnitudes of the hyperfine parameters inferred from the high-temperature analysis are gathered in

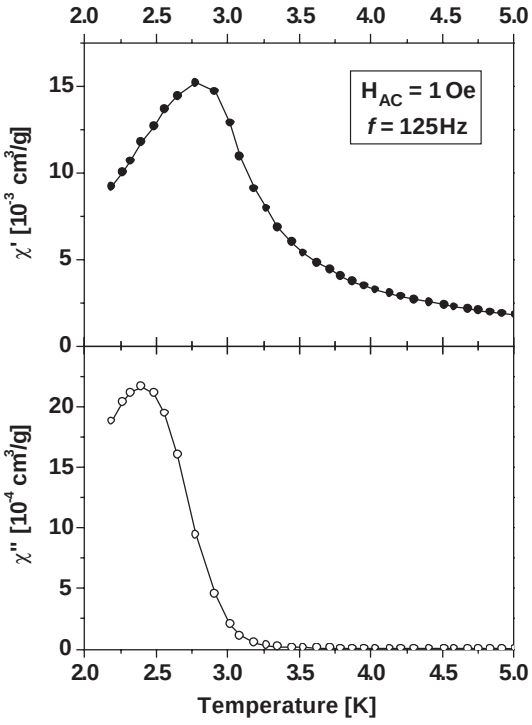

Fig. 4. Zero-field susceptibilities χ' and χ'' recorded simultaneously as a function of temperature with an oscillating field amplitude $H_{AC} = 1$ Oe at an internal frequency $f = 125$ Hz.

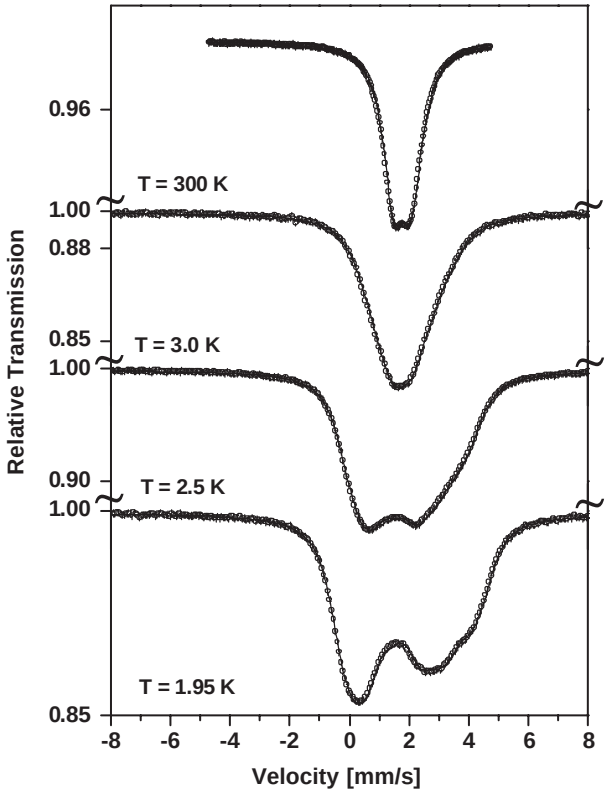

Fig. 5. Representative ^{119}Sn resonance spectra for PrRhSn at various temperatures. The continuous line is the least-squares fit to the experimental points.

Table 4
The hyperfine interaction parameters inferred from ^{119}Sn resonance spectra of PrRhSn in the paramagnetic state

T (K)	$\lvert\Delta E_Q^{\mathrm{eff}}\rvert$ (mm/s)	δ_{IS} (mm/s)	Γ (mm/s)	χ^2
300	1.18(1)	1.78(1)	0.82(1)	0.67
77	1.18(1)	1.79(1)	0.76(3)	0.69
4.2	1.17(2)	1.79(1)	0.99(2)	1.53

Table 4. Because of the low local symmetry of the tin sites, the asymmetry parameter η is different from zero. In this case only the effective quadrupole splitting parameter $|\Delta E_Q^{\mathrm{eff}}| = |eV_{zz}Q_g|(1+1/3\eta^2)^{1/2}$ can be experimentally determined. The absolute values of $\Delta E_Q^{\mathrm{eff}}$ are given because in the paramagnetic temperature range for $I_g = 1/2$ to $I_{ex} = 3/2$ gamma transition, the shape of the spectrum does not depend on the sign of the quadrupole interaction constant. Numerical analysis of the paramagnetic spectra allowed us to derive hyperfine parameters for PrRhSn at $T = 300\,\mathrm{K}$ as following: $|\Delta E_Q^{\mathrm{eff}}| = 1.11(2)\,\mathrm{mm/s}$, $\delta_{\mathrm{IS}} = 1.78(1)\,\mathrm{mm/s}$ and $\Gamma = 0.82(1)\,\mathrm{mm/s}$. The experimental absorption line widths Γ is almost equal to the theoretical value estimated, considering a small broadening of the source emission line and the broadening due to the finite absorber thickness.

As illustrated in Fig. 5, low temperature spectra measured around and below T_C have a more complicated shape due to magnetic splitting of the main doublet. Satisfactory fits for these spectra were made under few assumptions. First, the number of independently fitted parameters was reduced by constraining the absolute value of the effective quadrupole constant and the corresponding value of the half-width Γ to those obtained above the magnetic transition temperature. The quadrupole interaction constant ΔE_Q was calculated from the known magnitude of $\Delta E_Q^{\mathrm{eff}}$ and the fitted asymmetry parameter η (see Table 5). Secondly, both possible signs of ΔE_Q were checked. Only two sets of hyperfine parameters ($\Delta E_Q<0$ with $\varphi = 90^\circ$ and $\Delta E_Q>0$ with $\varphi = 0^\circ$) gave an asymmetry parameter η positive and lower than 1. Since the number of adjusted parameters was the same in both cases and because of the lower value of χ^2 for the fit with $\Delta E_Q<0$ and $\varphi = 90^\circ$, so then, this fit was chosen as the correct one. On the other hand, similar values were found for isostructural NdRhSn [7]. Thirdly, since the hyperfine lines were very broad and not well defined, it was necessary to use the method developed by Wivel and Mørup [18], which involves no assumptions concerning the shape of the distribution of hyperfine interaction parameters. Finally, spectra were effectively fitted with a single set of hyperfine parameters what will be explained later in the text.

Table 5
The hyperfine interaction parameters inferred from the low-temperature ^{119}Sn resonance spectra of PrRhSn

T (K)	ΔE_Q (mm/s)	δ_{IS} (mm/s)	θ (deg)	η	φ (deg)	Γ (mm/s)	χ^2
1.95	−0.98[a]	1.83(1)	78(2)	0.9(1)	90[a]	0.82[a]	1.21
2.25	−0.98[a]	1.83(1)	81(2)	0.8(1)	90[a]	0.82[a]	0.74
2.50	−0.98[a]	1.83(1)	90(10)	0.7(1)	90[a]	0.82[a]	0.79
2.75	−0.98[a]	1.83(1)	78[a]	0.9[a]	90[a]	0.82[a]	0.74
2.90	−0.98[a]	1.83(1)	78[a]	0.9[a]	90[a]	0.82[a]	0.87
3.00	−0.98[a]	1.82(1)	78[a]	0.9[a]	90[a]	0.82[a]	0.73
3.10	−0.98[a]	1.82(1)	78[a]	0.9[a]	90[a]	0.82[a]	0.74
3.25	−0.98[a]	1.81(1)	78[a]	0.9[a]	90[a]	0.82[a]	0.92
3.50	−0.98[a]	1.81(1)	78[a]	0.9[a]	90[a]	0.82[a]	0.95

[a]Parameters constrained during the fitting procedure.

The hyperfine parameters, i.e. the polar angle θ, the magnetic hyperfine field H_{hf} and the isomer shift δ_{IS} were varied independently. In the final step of the fitting procedure, the value of φ was constrained due to poor resolution of spectra.

In order to get more reliable information about the orientation of the EFG tensor with respect to the crystallographic axes we need to comment on some observations. The unit cell of PrRhSn contains three formula units with three equivalent tin atoms. The local symmetry of the tin sites has two mutually perpendicular mirror planes, where one plane lies in the *ab*-basal plane and the second one is parallel to the crystallographic *c*-axis. With each mirror plane one can associate the direction of the principal axis perpendicular to this plane. Therefore, one of the principal axes of the EFG tensor has to be parallel to the *c* axis and two others have to lie in the basal plane, with one of them parallel to the cross section of the mirror planes (site symmetry *m*2*m*). Then, with each of the three tin positions in the unit cell are associated three different principal systems of axes of the EFG tensor, which are equivalent after rotation around the *c*-axis by 120°. In this case, one can expect three magnetic components with different polar angles in the magnetically split Mössbauer spectrum. Taking the above remarks into account we started a fitting procedure with three well-defined components. Soon, it was clear that in this way we would not get satisfactory results.

Next, we tried to fit our data with the Czjzek–Berger method [21], where the average value $\langle H_{\mathrm{hf}}\rangle$ and the second moment of the field distribution were fitted as independent parameters. Nevertheless, spectra could not be reproduced in this manner. Therefore, the Wivel–Mørup approach [18] was applied. The probability distribution curves $F(H_{\mathrm{hf}})$ as a function of temperature are shown in Fig. 6. At first glance, one can see that this distribution function is divided into three weakly separated subsets and one low-field subset. The origin of the low-field component is not clear. Probably, it

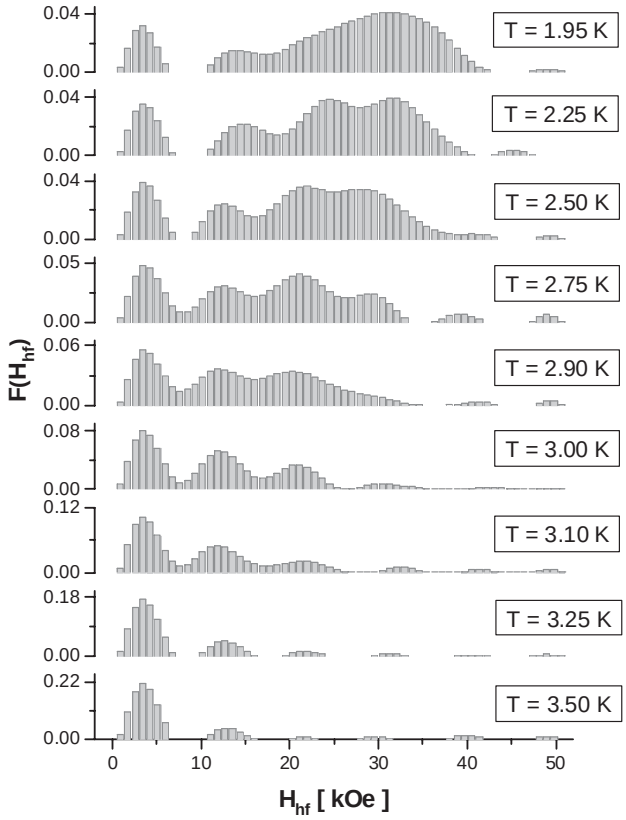

Fig. 6. Temperature evolution of the field distribution functions, $F(H_{hf})$, obtained from computer fits at various temperatures for PrRhSn. For explanation, see the main text.

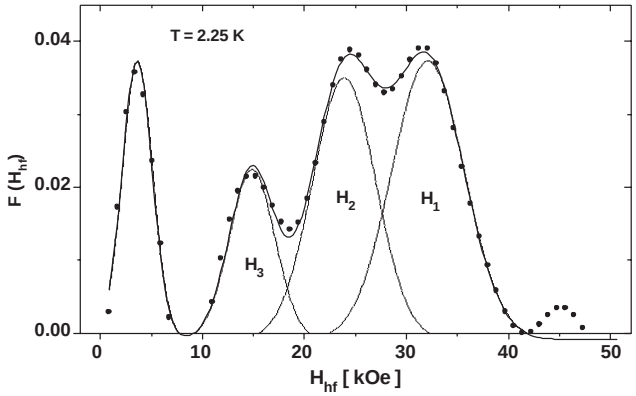

Fig. 7. Field distribution function $F(H_{hf})$ obtained at $T = 2.25$ K. Solid lines denote Gaussian profiles fitted to the distribution. Three main magnetic subsets are marked.

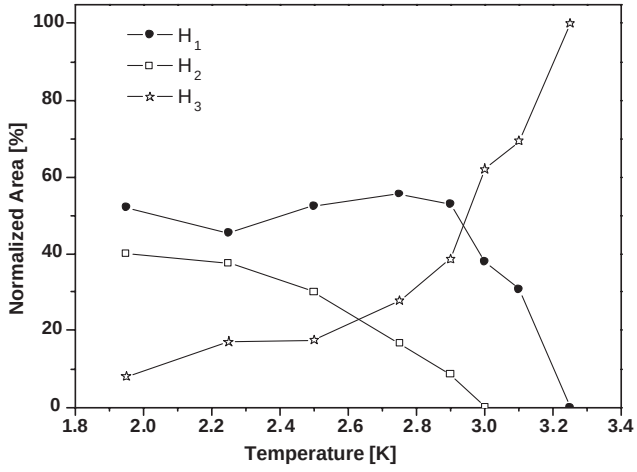

Fig. 8. Normalized areas of magnetic subsets as a function of temperature.

arises from small imperfections, i.e. swapping positions of tin and rhodium atoms, and it will not be discussed further. Weakly separated subsets correspond to the individual magnetic hyperfine fields, which might be characteristic for three different tin sites in a magnetic structure. It is clear that even at the lowest temperature the obtained distribution of the H_{hf} values is very wide and extends from $H_{hf} = 10$ to about 40 kOe. This was the main reason that other fitting methods were not efficient.

In order to get more information, our distribution curves were analyzed by Gaussian functions, which pretty well described the shapes of subsets (see Fig. 7). The normalized areas of three main magnetic components are shown in Fig. 8. This leads to the conclusion that components with high magnitudes of H_{hf} disappear close to the Curie temperature, whereas the third component still survives above T_C. Additionally, our analysis shows that some fractions of the sample with a higher value of the effective hyperfine field become larger with decreasing temperature at the cost of fractions having lower values of H_{hf}. It is a fingerprint of local differences in the way of magnetic ordering. All above observations point to a large magnetic inhomogeneity in the magnetic ordering of the praseodymium moments.

As was mentioned before the best fits were obtained for a negative value of ΔE_Q, $\varphi = 90^\circ$ and θ close to 80° (see Table 5). It has some implications concerning the direction of the praseodymium magnetic moments. For further analysis we need to specify the exact orientation of the principal axes of the EFG tensor with respect to the crystallographic axes. According to the discussion in Ref. [7] and references therein we choose the V_{yy} axis pointing along the c-axis and the V_{zz} axis lying in the ab-basal plane i.e. in the same way as it has been found for the isostructural compounds URhSn [22] and GdNiAl [23]. Similar procedure has recently been applied and it works also good for GdRhSn [5]. This particular choice of the alignment of the EFG principal axes system makes the interpretation of our Mössbauer results relatively simple. The derived values of the polar angles ($\varphi = 90^\circ$ and θ close to 80°) imply that the direction of the magnetic hyperfine field is not parallel to the c-axis but close to it. In this case, one can expect three

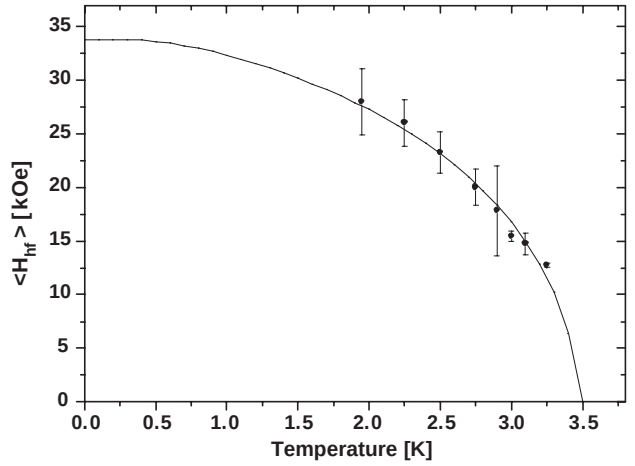

Fig. 9. Temperature dependence of the averaged magnetic hyperfine fields derived from computer fits to the ^{119}Sn Mössbauer spectra for PrRhSn. The continuous line represents the Brillouin-function, least-squares fit.

components with well-defined polar angles. As a matter of fact, the resonance spectra can be effectively described in terms of a single magnetic component with a unique set of polar angles but with a broad distribution.

Because the magnetic hyperfine field H_{hf} measured at the Sn site mainly comes from the transferred field, it is parallel to the magnetic moment of the rare earth (RKKY mechanism). Keeping all of this in mind, one can see that the direction of the praseodymium magnetic moments should be close to the crystallographic *c*-axis. In fact such a preference of the praseodymium magnetic moment direction has already been anticipated from ^{155}Gd Mössbauer results obtained for GdRhSn [5] being self-consistent with the whole analysis presented up to now.

The temperature dependence of the averaged magnetic hyperfine field $\langle H_{hf}(T)\rangle$ (Fig. 9) can be well described in the frame of molecular field approximation by a Brillouin function with $J = 4$ for the Pr^{3+} ion. The resulting fit gives an estimation for the Curie temperature $T_C^M = 3.5(1)\,K$ which is slightly larger than that obtained from the magnetic DC measurements $T_C = 3.0\,K$. The absolute value of the saturated magnetic hyperfine field $|H_{hf}(0)|$ is 33.8(1) kOe.

The value of the tin isomer shift (see Table 5) is almost temperature independent and is typical for tin atoms in other intermetallic systems as for example observed in NdRhSn [7] and GdRhSn [5].

4. Conclusions

The powder and single crystal X-ray diffraction data revealed that the structure of PrRhSn is isotypic with the hexagonal ZrNiAl type [10–12], space group $P\bar{6}2m$. Bulk magnetic AC and DC measurements have shown that this compound is ferromagnetic with a Curie temperature of $T_C = 3.0\,K$. The thermal variation of the hyperfine parameters has been studied in detail by ^{119}Sn Mössbauer spectroscopy. Especially, the large distribution of magnetic hyperfine fields observed at the tin sites points to a rather complicated magnetic structure of a probably non-collinear character but with the magnetic praseodymium moments arranged in directions close to *c*-axis. Ferromagnetic PrRhSn nicely completes the series of magnetic RERhSn stannides, where outstanding materials like valence fluctuating CeRhSn or the heavy fermion compound YbRhSn have been observed.

Acknowledgments

We are grateful to the Degussa-Hüls AG for a gift of rhodium powder, to H.J. Göcke for the work at the scanning electron microscope, and to Dr. R.-D. Hoffmann for the intensity data collection. This work was supported by the Deutsche Forschungsgemeinschaft through SPP 1166 *Lanthanoidspezifische Funktionalitäten in Molekül und Material* and by Poland's Committee for Scientific Research grant under contract No: 1 P03B 084 28. K.L. is indebted to the Deutsche Forschungsgemeinschaft for a research grant.

References

[1] R. Mishra, R. Pöttgen, R.-D. Hoffmann, H. Trill, B.D. Mosel, H. Piotrowski, M.F. Zumdick, Z. Naturforsch. 56b (2001) 589.
[2] A. Schenk, F.N. Gygax, M.S. Kim, T. Takabatake, J. Phys. Soc. Jpn 73 (2004) 3099.
[3] A. Ślebarski, T. Zawada, J. Spałek, A. Jezierski, Phys. Rev. B 70 (2004) 235112.
[4] H. Tou, M.S. Kim, T. Takabatake, M. Sera, Phys. Rev. B 70 (2004) 100407.
[5] K. Łątka, R. Kmieć, R. Kruk, T. Pacyna, Th. Fickenscher, R.-D. Hoffmann, R. Pöttgen, J. Solid State Chem. 178 (2005) 2077.
[6] Ch.D. Routsi, J.K. Yakinthos, H. Gamari-Seale, J. Magn. Magn. Mater. 117 (1992) 79.
[7] K. Łątka, R. Kmieć, J. Gurgul, A.W. Pacyna, M. Rams, T. Schmidt, R. Pöttgen, J. Magn. Magn. Mater., in press.
[8] R. Pöttgen, Th. Gulden, A. Simon, GIT Labor-Fachzeitschrift 43 (1999) 133.
[9] K. Yvon, W. Jeitschko, E. Parthé, J. Appl. Crystallogr. 10 (1977) 73.
[10] P.I. Krypyakevich, V.Ya. Markiv, E.V. Melnyk, Dopov. Akad. Nauk. Ukr. RSR, Ser. A (1967) 750.
[11] A.E. Dwight, M.H. Mueller, R.A. Conner Jr., J.W. Downey, H. Knott, Trans. Met. Soc. AIME 242 (1968) 2075.
[12] M.F. Zumdick, R.-D. Hoffmann, R. Pöttgen, Z. Naturforsch. 54 (1999) 45.
[13] G.M. Sheldrick, SHELXL-97, Program for Crystal Structure Refinement, University of Göttingen, 1997.
[14] H.D. Flack, G. Bernadinelli, Acta Crystallogr. A 55 (1999) 908.

[15] H.D. Flack, G. Bernadinelli, J. Appl. Crystallogr. 33 (2000) 1143.
[16] G. Czjzek, Mössbauer Spektroskopie: Optimale Absorberdicke, unpublished.
[17] R. Kmieć, Ż. Świątkowska, R. Kruk, K. Tomala, J. Magn. Magn. Mater. 271 (2004) 326.
[18] C. Wivel, S. Mørup, J. Phys. E 14 (1981) 605.
[19] J. Emsley, The Elements, Clarendon Press, Oxford, 1989.
[20] Ch.D. Routsi, J.K. Yakinthos, H. Gamari-Seale, J. Magn. Magn. Mater. 110 (1992) 317.
[21] G. Czjzek, W.G. Berger, Phys. Rev. B 1 (1970) 957.
[22] R. Kruk, R. Kmieć, K. Łątka, K. Tomala, R. Troć, V.H. Tran, Phys. Rev. B 55 (1997) 5851.
[23] J. Gurgul, Thesis, Institute of Physics, Jagiellonian University, Poland, 2002.